

1 **Dimensionality reduction by UMAP reinforces sample heterogeneity analysis in bulk
2 transcriptomic data**

3

4 Yang Yang^{1,2}, Hongjian Sun^{2,3}, Yu Zhang⁴, Tiefu Zhang⁵, Jialei Gong⁶, Yunbo Wei⁴, Yong-Gang
5 Duan⁶, Minglei Shu², Yuchen Yang^{7,8}, Di Wu^{*9}, Di Yu^{*1,2,4}

6

7 ¹ The University of Queensland Diamantina Institute, Translational Research Institute, Faculty of
8 Medicine, The University of Queensland, Brisbane, Australia

9 ² Shandong Artificial Intelligence Institute, Qilu University of Technology (Shandong Academy of
10 Sciences), Jinan, China

11 ³ School of Microelectronics, Shandong University, Jinan, China

12 ⁴ Laboratory of Immunology for Environment and Health, School of Pharmaceutical Sciences, Qilu
13 University of Technology (Shandong Academy of Sciences), Jinan, China

14 ⁵ University of Electronic Science and Technology of China, Chengdu, China

15 ⁶ Shenzhen Key Laboratory of Fertility Regulation, Center of Assisted Reproduction and Embryology,
16 the University of Hong Kong - Shenzhen Hospital, Shenzhen, China

17 ⁷Department of Pathology and Laboratory Medicine, University of North Carolina at Chapel Hill,
18 Chapel Hill, USA

19 ⁸McAllister Heart Institute, University of North Carolina at Chapel Hill, Chapel Hill, USA

20 ⁹ Department of Biostatistics, University of North Carolina at Chapel Hill, Chapel Hill, USA

21 ***Corresponding author:**

22 **Di Yu**

23 The University of Queensland Diamantina Institute, Translational Research Institute, Faculty of
24 Medicine, The University of Queensland, Brisbane, Australia.

25 E-mail address: di.yu@uq.edu.au

26 **Di Wu**

27 Department of Biostatistics, University of North Carolina at Chapel Hill, Chapel Hill, USA

28 E-mail address: dwu@unc.edu

29

30 **Abstract**

31 Transcriptome profiling and differential gene expression constitute a ubiquitous tool in biomedical
32 research and clinical application. Linear dimensionality reduction methods especially principal
33 component analysis (PCA) are widely used in detecting sample-to-sample heterogeneity in bulk
34 transcriptomic datasets so that appropriate analytic methods can be used to correct batch effects,
35 remove outliers and distinguish subgroups. In response to the challenge in analysing transcriptomic
36 datasets with large sample size such as single-cell RNA-sequencing (scRNA-seq), non-linear
37 dimensionality reduction methods were developed. t-distributed stochastic neighbour embedding (t-
38 SNE) and uniform manifold approximation and projection (UMAP) show the advantage of preserving
39 local information among samples and enable effective identification of heterogeneity and efficient
40 organisation of clusters in scRNA-seq analysis. However, the utility of t-SNE and UMAP in bulk
41 transcriptomic analysis has not been carefully examined. Therefore, we compared major
42 dimensionality reduction methods (linear: PCA; nonlinear: multidimensional scaling (MDS), t-SNE,
43 and UMAP) in analysing 71 bulk transcriptomic datasets with large sample sizes. UMAP was found
44 superior in preserving sample level neighbourhood information and maintaining clustering accuracy,
45 thus conspicuously differentiating batch effects, identifying pre-defined biological groups and
46 revealing in-depth clustering structures. We further verified that new clustering structures visualised
47 by UMAP were associated with biological features and clinical meaning. Therefore, we recommend
48 the adoption of UMAP in visualising and analysing of sizable bulk transcriptomic datasets.

49

50 **Introduction**

51 Bulk transcriptome profiling quantifies the transcripts in a given biological sample, achieved by
52 technologies including microarray [1, 2] and RNA sequencing (RNA-seq) [3, 4]. This tool is
53 ubiquitously adopted in modern biomedical research and application to reveal unique features of gene
54 expression for specific cell or tissue type and biological process. The principal task of bulk
55 transcriptome profiling is to analyse differential gene expression (DGE) of samples between biological
56 groups. When statistically modelling DGE, an implicit assumption is that data of individual samples
57 within a given group are relatively homogeneous. For instance, to investigate the biomarker for a
58 certain disease, the group comparison between patient and healthy control cohorts presumes that the
59 biological characteristics of individual patients are largely indistinguishable when compared to healthy
60 controls, and vice versa. However, there exists heterogeneity within a group, which can lie in samples'
61 distinct biological states. For example, patients with systemic lupus erythematosus (SLE) show distinct
62 disease activities and can be classified based on the levels of disease activity index [5]. Other
63 heterogeneity can result from different sample preparation or processing conditions, often referred to
64 as batch effects [6, 7]. Therefore, it is crucial to scrutinise sample-to-sample heterogeneity within
65 groups so that subgroups or outliers can be identified. Only with such information, appropriate analytic
66 methods can be used to correct batch effects, remove outliers and distinguish subgroups. In contrast,
67 DGE analysis simply in given groups without the knowledge of sample-to-sample heterogeneity within
68 groups can often lead to biased or even wrong conclusion.

69 To detect among-sample heterogeneity in bulk transcriptome profiling, individual samples are
70 visualised in embedded space by dimensionality reduction methods. Principal component analysis
71 (PCA, [8]) and multidimensional scaling (MDS, [9]) have been thoroughly exploited to obtain an
72 overview of sample relationship in a low-dimensional space [10-13]. Both methods succeeded in
73 visualising biological or technical variation among samples by uncovering the overall structure of the
74 sample-to-sample relationship, which represents the key information of among-sample heterogeneity.

75 Since 2009 [14], the new era of characterising transcriptome at single-cell level has arrived. Numerous
76 single-cell RNA sequencing (scRNA-seq) technologies enable simultaneous profiling of thousands of
77 cells' transcriptomes in a given sample so that the analysis of population heterogeneity can identify
78 complex compositions, reveal rare cell populations, detect differentially expressed genes between
79 multiple cell populations or between samples for cell types, uncover cell differentiation trajectories,
80 and so forth [15, 16]. However, PCA and MDS show inefficient performance for dimensionality
81 reduction of scRNA-seq data while two non-linear methods, *t*-distributed stochastic neighbour

82 embedding (*t*-SNE) [17] and uniform manifold approximation and projection (UMAP) [18, 19] exhibit
83 better capability due to the advantage of maintaining cell-to-cell neighbour information and visualising
84 local structure. Compared to *t*-SNE, UMAP can not only distinguish neighbouring clusters but also
85 retain the global structure in scRNA-seq data analysis [18, 19].

86 The continuous improvement and invention of sequencing platforms has hugely improved the
87 efficiency and throughput of DNA sequencing and resulted in a dramatic reduction in costs, which
88 enable to generate a large number of samples and datasets of bulk transcriptome profiling. For example,
89 the landmark cancer genomics program – The Cancer Genome Atlas (TCGA) has profiled over 20,000
90 primary cancer and matched normal samples spanning 33 cancer types and generated over 2.5
91 petabytes of genomic, epigenomic, transcriptomic, and proteomic data [20-22]. While PCA remains
92 as the mainstream tool recommended detecting among-sample heterogeneity in bulk transcriptome
93 profiling, such as by TCGA Batch Effects [6, 7], we hypothesis that, for datasets with large sample
94 sizes, local structure of sample-to-sample relationship becomes more prominent for sample
95 heterogeneity analysis. Therefore, non-linear methods *t*-SNE and UMAP might outperform PCA and
96 MDS.

97 In this study, we visually and quantitatively compared the capabilities of PCA, MDS, *t*-SNE, and
98 UMAP in heterogeneity exploration of bulk transcriptome profiling. By visualising and interpreting
99 71 sizeable datasets of bulk transcriptome profiling, we found that UMAP was superior in preserving
100 sample level neighbourhood information and maintaining clustering accuracy, thus conspicuously
101 differentiating batch effects, identifying pre-defined biological groups and identifying new clustering
102 structures associated with biological features and clinical meaning.

103

104 **Result**

105 *Overview of the evaluation*

106 The bulk-transcriptome profiling datasets were collected from the Gene Expression Omnibus (GEO)
107 database within past five years (**Table S1**). To minimize the cell type effects interacting with our
108 results which are usually strong and very easy to be identified, we only chose the datasets of human
109 samples from peripheral blood mononuclear cells (PBMCs) or whole blood for bulk transcriptome
110 analysis, that are among most frequent cell populations. Datasets with the size less than 100 samples
111 were excluded in order to generate observable and meaningful clusters. The collection covered a
112 diverse range of biomedical research including the investigations on disease features such as SLE [23-]

113 29] and influenza infection [30-32], and the evaluation on interventions such as therapies and
114 vaccination [33-37].

115 The research design flowchart is shown in **Figure 1a**. Among a total collection of 71 datasets based
116 on the above procedure, there were 41 datasets revealing clustering structures in plots of two-
117 dimensional embedding space by the dimensionality reduction methods PCA, MDS, t-SNE and UMAP.
118 UMAP reported all clustering (41/71) and, together with t-SNE (37/71), performed significantly better
119 than PCA (11/71) and MDS (13/71) (**Figure 1b**). The 41 datasets were classified into three categories
120 by incorporating available features (**Figure 1b**). As in **Figure 1b**, three plots in the two-dimensional
121 embedding space from the dimension reduction methods showed clusters related to batches (batch
122 effect) described in studies for these datasets while 9 plots showed clusters related to biological groups
123 designated by study designs. In addition, 29 plots revealed new clustering not related to batch
124 information or biological group by study design, suggesting significant sample-to-sample
125 heterogeneity in bulk transcriptome analysis. We identified the relationship of new clustering
126 structures with known sample features for 9 plots. The clustering structures of the rest of 20 plots could
127 result from hidden batch effect or biological features not reported by publications, thus referred to as
128 new clustering with hidden features (**Figure 1b**).

129 With clustering structures generated by PCA, MDS, t-SNE and UMAP, we could evaluate individual
130 methods' performance for clustering accuracy, local information preservation, and computational
131 efficiency. For datasets with clustering structure by batch effect or biological group, we would then
132 compare the separability of each method in detecting distinct groups. For new clustering structures,
133 we would investigate the relationships of clustering structures with sample features. Based on these
134 quantitative and qualitative assessments, we could provide the recommendation of the best performing
135 method for dimensionality reduction in sizeable bulk transcriptome analysis (**Figure 1a**).
136

137 ***Comparison of dimensionality reduction methods by quantitative analysis***

138 *Clustering accuracy*

139 The foremost objective of dimensionality reduction for bulk transcriptomic analysis is to
140 conspicuously distinguish clustering structures of samples which associate biological meaning. We
141 applied five clustering algorithms (k-means, hierarchical clustering, spectral clustering, Gaussian
142 mixture model and hdbscan, with details of five algorithms in **Table S3**) to low-dimensional spaces
143 projected by dimensionality reduction methods and compared the clustering accuracy.

144 The five clustering algorithms were performed on the embedding two-dimensional coordinates of 22
145 datasets which have available label information for groups (labelled in **Table S1**). To assess clustering
146 accuracy of dimensionality reduction methods, we then computed Normalized Mutual Information
147 (NMI) [38] and Adjusted Rand Index (ARI) [39] for comparing the true group labels and inferred
148 group labels obtained by clustering algorithms based on the low-dimensional components, and the
149 lager score indicates better clustering accuracy. UMAP was scored the highest for both NMI and ARI,
150 no matter what clustering algorithm used, achieving the best accuracy for clustering (**Figure 2a** and
151 **S1**). t-SNE was scored slightly lower than UMAP but well outperformed MDS and PCA (**Figure 2a**
152 and **S1**).

153 *Neighbourhood preserving*

154 We then evaluated the performance of different dimensionality reduction methods in retaining local
155 information from original datasets, which was assessed by comparing the fidelity of local
156 neighbourhood structures between the reduced low-dimensional space and the original space using a
157 Jaccard index (details in ‘Methods’) [40] . The Jaccard indexes were computed for 15 neighbours
158 (**Figure 2b**) and 30 neighbours (**Figure S2**), respectively. PCA exhibited the worst performance in
159 preserving neighbourhood information (averaged 0.19 ± 0.067), followed by MDS (averaged $0.26 \pm$
160 0.114). The performance of UMAP (averaged 0.35 ± 0.091) appeared comparable to that of t-SNE
161 (averaged 0.36 ± 0.095), and both were better than PCA and MDS. Pairwise t-test was performed
162 between every two methods (**Figure 2b**), and statistically significant differences were detected
163 between group means by one-way ANOVA ($F(3, 280) = 57.88$, $p < 0.001$). This was conceivable
164 since UMAP and t-SNE are designed to utilise local information for dimensionality reduction.

165 *Computational efficiency*

166 We next measured the execution time of each dimensionality reduction method on data with sample
167 size ranging from 200 to 10,000. The varied scales of data were generated by randomly sampling with
168 replacement from the three largest datasets (GSE36382, GSE65391 and GSE65907). As shown in
169 **Figure 2c**, the variability of consumed time among different datasets was negligible. PCA performed
170 consistently faster than the other three methods while MDS ran slowest (**Figure 2c**). For 200 and 500
171 samples, consumed time was similar between t-SNE and UMAP but UMAP gained an advantage for
172 data with larger sample sizes. For processing a data with 10,000 samples, UMAP (~3 minutes) was
173 more than 25-time faster than t-SNE (~ 1.5 hours), although still slower than PCA (~20 seconds)
174 (**Figure 2c**). PCA and UMAP appeared more time-efficient than MDS and t-SNE for computing large-
175 sized data.

176 Technically, UMAP not only identified more clustering structure in 71 datasets of bulk transcriptome
177 analysis (**Figure 1b**), but was also superior to the other three methods for the overall performance by
178 assessing the three quantitative criteria. We next compared four dimensionality reduction methods for
179 uncovering biological meaning.

180

181 ***Comparison of dimensionality reduction methods by qualitative analysis***

182 *Identification of batch effects*

183 Batch effects are common in many types of high-throughput sequencing experiments, which are
184 systematic technical variations introduced by processing samples in different batches [6, 41]. As for
185 high-throughput sequencing experiments, it is essential to remove unwanted variations in the
186 transcriptomic analysis by normalisation [42, 43] to avoid biased analysis and distorted results [6]. The
187 first step is to identify batch effects among samples. PCA is the most used tool, such as by The Cancer
188 Genome Atlas (TCGA) project [21]. It generates the clustering structure of samples in two-
189 dimensional embedding space to facilitate the visualisation for batch information. Among the 41
190 datasets with explicit clustering structures, three datasets showed clustering structures related to batch
191 effects reported by publications (**Figure 1b**). Each dimensionality reduction method was used to
192 visualise batch effects for the three datasets (one in **Figure 3a** and two in **S3**). UMAP and t-SNE
193 showed better segregation between samples from different batches. To assess the ability of each
194 method to separate batch effects in two-dimensional embeddings, we trained random forests to predict
195 batch effects from sample points in embedding space and calculated the prediction accuracy on held-
196 out data (details in ‘Method’). Consistent with the visualisation, UMAP and t-SNE performed better
197 than MDS and PCA, leading to random-forest accuracies around 90% (**Figure 3b**).

198 *Validation of biological groups by experimental design*

199 One major purpose of bulk transcriptome analysis is for the DGE analysis between biological groups
200 defined by experimental design. Visualising the segregation of samples from groups with distinct
201 biological features by dimensionality reduction is often applied to the validation of group-to-group
202 distinction. Among the 41 datasets with explicit clustering structures, 9 datasets showed clustering
203 structures related to biological groups by experimental designs (**Figure 1b**). We compared four
204 dimensionality reduction methods in visualizing biological group and found that UMAP and t-SNE
205 outperformed MDS or PCA in visually separating biological groups in 9 datasets (one in **Figure 3c**
206 and eight in **S4**). To measure the separability of each method in group validation, we again deployed
207 random forests to train embedding data with group features as labels and computed the prediction

208 accuracy on held-out data (details in ‘Method’). UMAP achieved the best accuracy (> 80%) than t-
209 SNE ($p < 0.05$), MDS ($p < 0.001$) and PCA ($p < 0.001$) in separating biological groups (**Figure 3d**).

210 *Uncovering new associations between clustering structures and sample features*

211 Only 12 out of 41 datasets showed clustering structures explained by batch effects or biological groups
212 (**Figure 1b**). The appearance of new clustering structures in 29 plots demonstrated significant
213 heterogeneity existing in bulk transcriptome profiling, which could be efficiently revealed by UMAP.
214 We next investigated the causes underlying new clustering structures. The clustering structures in 9
215 datasets were found associated with certain sample features reported by publications (**Figure S5**).
216 These features were not used for the classification of sample groups in experimental designs,
217 suggesting certain biological features with major impacts on sample heterogeneity were not included
218 in experimental designs or data analyses. A good case was the dataset GSE71220, which was designed
219 to determine the impact of cigarette smoking (former v.s. current smoker) on gene expression in
220 peripheral blood of patients with chronic obstructive pulmonary diseases (COPD) [44]. Dimensionality
221 reduction methods of UMAP and t-SNE generated plots showing clustering structures (right part in
222 **Figure 4a**). However, such clustering was not associated with smoking status (**Figure 4b**). We applied
223 other sample features including age and disease status to the two-dimensional plots. Surprisingly, the
224 sample feature of gender demonstrated clear association with clusters in the plots generated by UMAP
225 and, to less extent, t-SNE (**Figure 4c**). In the UMAP plot, one cluster was highly enriched of females
226 (in orange colour) and another cluster was highly enriched by males (in blue colour), with the third
227 cluster showing the pattern of a mixture (**Figure 4c**). By deploying spectral clustering (details in
228 ‘Methods’), samples were divided into three clusters with distinct gender composition: C1-97%
229 females, C2-93% males, and C3-mixed (**Figure 4d, e**). This indicated that the transcriptomes of
230 samples in this study were highly influenced by gender difference. Indeed, the heatmap of the top 100
231 differentially expressed genes demonstrated that the clustering of samples was strongly associated with
232 gender (**Figure 4f**). Therefore, the heterogeneity uncovered by the dimensionality reduction using
233 UMAP indicated that the gender difference should have been critically treated as a latent variable in
234 downstream transcriptomic analysis.

235 *Discovering new associations between clustering structures and hidden features*

236 By dimensionality reduction using UMAP, 41 datasets showed clustering structures in two-
237 dimensional embedding spaces in which the associations with batch effects, biological groups by
238 experimental designs or specific sample features reported by publications were identified in 21 datasets
239 (**Figure 1b**). For the rest 20 datasets, clustering structures might derive from obscure heterogeneity of

240 samples, biologically or technically (**Figure S6**). We made efforts to explore the biological meanings
241 of clustering structures of these datasets and herein present the dataset GSE121239 as an example to
242 support the notion that new clustering structures generated by UMAP can reinforce sample
243 heterogeneity analysis of bulk transcriptome data to reveal important biological meaning.

244 Dataset GSE121239 originated from the study of systemic lupus erythematosus (SLE) which is the
245 prototype of systemic autoimmune diseases with highly diverse manifestations in multiple tissues and
246 organs, such as skin, kidney and lung [45]. As a chronic disease, SLE patients often experience
247 unpredictable occurrence of disease flares [46]. In order to identify the heterogeneity of SLE patients
248 and stratify patient groups of disease activity progression, the dataset GSE121239 collected
249 longitudinal transcriptome profiles of 65 SLE patients with more than three clinical visits and 20
250 healthy individuals as controls [47]. Data collected at each visit contributed to one sample in the dataset.
251 Dimensionality reductions plot by UMAP and t-SNE, but not PCA or MDS, demonstrated clearly
252 separated clusters for SLE patients (in orange colour) and healthy controls (in blue colour) (**Figure 5a, b**). In the UMAP plot, we noticed more than one cluster for patient samples (**Figure 5c**). To understand
253 the biological meaning of clusters representing subgroups of SLE patients, we examined feature
254 information of patients reported by the publication including gender and patient ID but found no direct
255 association with the clustering structure of patient subgroups. Since the samples of patients were
256 collected longitudinally from multiple clinical visits, we set samples collected at the first clinical visit
257 as day 1 then labelled subsequently collected samples from the same patient with the period between
258 two visits. The resulted contour plot showed samples in the chronological order (**Figure 5d**). Importantly,
259 the gradient from light to dark orange spreads from the middle of the plot to two sides, indicating
260 the clustering structure generated by UMAP was associated with the timing evolution of
261 clinical visits. For example, the bottom-right cluster in **Figure 5c** represents samples collected from a
262 subgroup of patients at their late clinical visits, indicated by dark orange in **Figure 5d**. This intriguing
263 discovery suggested that new clustering structures revealed by UMAP could facilitate the exploration
264 of samples' hidden features.

266 To generate UMAP plots, there are several options for metric space, with '*euclidean*' distance as
267 default [18]. We tested '*euclidean*' and another two representative metrics '*canberra*' and '*cosine*' and
268 observed that the metric '*canberra*' led to more explicit clustering on UMAP projection, with patients'
269 samples clustered into three subgroups: sG0, sG1, sG2 (**Figure 5e**).

270 According to the timing evolution (**Figure 5d**), samples of sG0 were collected earlier while samples
271 of sG1 or sG2 were collected later. The clear separation of late collected samples into two clusters of
272 sG1 and sG2 suggested a biological divergence. To interpret the biological difference between sG1

273 and sG2, we applied gene set enrichment analysis (GSEA) using R package EGSEA [48], resulting in
274 the top 20 differentially regulated molecular pathways between sG1 v.s. sG0 and sG2 v.s. sG0 (**Figure**
275 **6b, S7**). Comparing to sG0, sG1 and sG2 were common in 6 upregulated pathways (in red colour) and
276 2 down-regulated pathways (in blue colour). However, 7 upregulated and 5 downregulated pathways
277 in sG1 showed opposite trends in sG2, suggesting the biological distinction between them.
278 Given longitudinal sampling of individual patients, we next investigated the visit trajectories of
279 individual patients. Connection of samples from each patient demonstrated that most patients ($N =$
280 47/65) showed one-directional trajectories from sG0 to sG1 or sG0 to sG2 (**Figure 6c**), in agreement
281 with the timing evolution of patients' sample (**Figure 5d**). When initially admitted to the clinic to take
282 samples (visit 1, **Figure 6d**), patients with distinct trajectories had comparable disease activities (SLE
283 disease activity index (SLEDAI), mean \pm SD, sG0 to sG1: 2.6 ± 2.71 ; sG0 to sG2: 2.6 ± 2.85). Widely
284 used in clinical practice and research, SLEDAI is a global index that was developed as a clinical index
285 for the assessment of lupus disease activity and larger SLEDAI indicates worse disease conditions [5].
286 Importantly, we noticed that the average SLEDAI at the following visits increased for patients with
287 the trajectory from sG0 to sG1 (in blue colour, **Figure 6d**), indicating the disease deterioration of these
288 patients, whereas the average SLEDAI at the following visits decreased for patients with the trajectory
289 from sG0 to sG2 (in green colour, **Figure 6d**), indicating the disease improvement of these patients.
290 The opposite disease progression between two trajectories was also supported by GSEA, which
291 showed the key pathogenic pathways for SLE including apoptosis [49], type I interferon [50] and type
292 II interferon [51] were increased in sG1 but decreased in sG2 (**Figure 6b**). Taken together, the deep
293 exploration of the biological and clinical meaning of the new clustering structure of dataset
294 GSE121239 revealed by UMAP supports the future application of dimensionality reduction methods
295 such as UMAP to reinforce sample heterogeneity analysis of bulk transcriptome data.
296

297 ***Recommendation***

298 Although PCA is often used in identifying sample-to-sample heterogeneity in bulk transcriptome
299 analysis, our study demonstrated that the nonlinear dimensionality reduction method UMAP improved
300 the identification, visualisation and interpretation of clustering structures in sizeable datasets. The
301 analysis of the dataset GSE121239 suggested that the choice of the parameter '*metric*' in UMAP could
302 affect the visualisation of clustering structures of UMAP plots (**Figure 6a**). We then thoroughly
303 evaluate '*euclidean*', '*canberra*' and '*cosine*' metrics of UMAP in all 71 bulk transcriptomic datasets,
304 which respectively revealed clustering structures in 41, 44 and 42 datasets and had 39 datasets in
305 common (**Figure 7a**). Without any '*metric*' showing a clear advantage, we recommend trying the three

306 representative metrics for UMAP in visualising the bulk transcriptomic data and being integrated into
307 the pipeline for bulk transcriptomic analysis (**Figure 7b**). The analysis starts with transcript counts as
308 the input, followed by applying UMAP to visualise potential clustering structures. If no clustering
309 structure is detected, DGE analysis can be performed. With clustering structures that may correspond
310 to known or unknown batch effects, the first consideration is to identify and remove batch effects. The
311 clustering structure should next be tested for the association with biological groups assigned by
312 experimental design. The explicit association of the clustering structure with biological groups can
313 ensure robust DGE analysis among different biological groups. If the clustering structure is related to
314 specific sample features rather than biological groups, that feature should be treated as latent covariates
315 in DGE analysis. On the other hand, the clustering structure might reveal new biological subgroups or
316 hidden factor to be analysed separately for DGE analysis.

317

318 **Discussion**

319 Sample heterogeneity in bulk transcriptomic data reflects both biological and technical variation
320 among samples. It is crucial to detect among-sample heterogeneity before DGE analysis for bulk
321 transcriptomic data so that appropriate analytic methods can be subsequently used to correct batch
322 effects, remove outliers and distinguish subgroups. Sample heterogeneity analysis by dimensionality
323 reduction should consider both local and global information of datasets to congregate similar samples
324 and distinguish different samples. PCA is the current mainstream tool of dimensionality reduction to
325 visualise and detect among-sample heterogeneity, adopted by widely used analytic packages limma
326 and edgeR [11, 12]. PCA produces linear combinations of the original variables to generate the
327 principal components [52], and visualisation is generated by projecting the original data to the first
328 two principal components, thus PCA plot linearly shows global distance among data points. Similarly,
329 MDS method places each data point into two-dimensional space such that the between-point distances
330 are preserved according to the pairwise distance of original data points [53]. Both PCA and MDS focus
331 more on maintaining global information, which can fail to compactly cluster similar data points and
332 face a major challenge with the rapid increase in sample sizes of bulk transcriptomic profiling datasets.

333 On the other hand, t-SNE and UMAP model the pairwise distance by adopting the concept from k-
334 nearest neighbour (kNN) graph [17, 18] whereby two points are connected by an edge if their distance
335 is among the k-th smallest distances compared to distances to other points [54]. For dimensionality
336 reduction by t-SNE or UMAP, all pairs of two points have edge weights indicating the probability for
337 them being connected (connection probability). If the distance between two points is among the k-th
338 smallest distances compared to distances to other points, the connection probability between these two

339 points is high. If the distance between two points is much greater than the k-th smallest distance, the
340 connection probability between these two points is low [17, 18]. Therefore, t-SNE and UMAP can
341 efficiently preserve local distance information and cluster similar sample points. For large sample size
342 in dataset resulting in the quadratic increase of pairwise comparisons, t-SNE and UMAP not only
343 retain pairwise interaction but also focus on local information, thus outperforming PCA and MDS in
344 detecting sample heterogeneity. Compared with t-SNE using random initialisation and KL-divergence
345 object function, UMAP utilises Laplacian Eigenmaps initialisation and cross-entropy object function
346 [18, 55] which contribute to the global structure preservation. This might explain the overall better
347 performance of UMAP than t-SNE. We tested three presentative parameters for the distance '*metric*'
348 of UMAP – '*euclidean*', '*canberra*' and '*cosine*' and found consistent outcomes with only minor
349 variation (**Figure 7a**).

350 Among 71 bulk transcriptome profiling datasets with > 100 samples tested in this study, UMAP and
351 t-SNE clearly outperformed PCA and MDS in identifying clusters associated with batch effects and
352 biological groups pre-defined in study designs. It should be noted that, within 41 of 71 datasets that
353 UMAP identified clustering structures, new fine-scale clustering structures were revealed and
354 accounted for more than half (29 out of 41) (**Figure 1**). The important question is whether the new
355 clustering structures discovered by UMAP represent biological significance. This question was then
356 addressed in case studies of datasets with new clustering structures. One case is the study that was
357 initially designed to investigate how smoking influence blood gene expression of patients with COPD
358 and utilised bulk transcriptomic profiling and DGE analysis (GSE71220 [44]). Intriguingly, the PCA
359 plot showed no clustering structure while the UMAP plot revealed new clustering structures, which
360 was related to gender rather than smoking status (**Figure 4**). This information discovered by
361 dimensionality reduction using UMAP suggests the gender feature should be treated as an important
362 latent covariate in DGE analysis. Another example is the study that was designed to stratify patients
363 with SLE, a highly complex autoimmune disease with heterogeneous clinical presentation, according
364 to longitudinal disease activity and blood gene expression (GSE121239 [47]). This study calculated a
365 gene-by-patient correlation matrix computing a stringent Pearson correlation coefficient between gene
366 expression data and SLEDAI scores across each patient's visits and then selected genes with the highest
367 absolute correlation values by rank-sum method [47]. Instead of this multiple-step process, dimension
368 reduction by UMAP revealed the separation of samples by visit timestamp (**Figure 5**), which enabled
369 to identify two groups of patients with opposite changes of longitudinal disease activity (**Figure 6**).
370 These results thus validate the application of UMAP in dimensionality reduction in stratifying SLE
371 patients. Using several datasets as examples, we demonstrated that the new clustering structures were

372 associated with certain sample features and enabled to uncover unappreciated sample subgroups with
373 specific biological and clinical features.

374 In analysing 71 datasets, we demonstrated that UMAP was able to visualise the among-sample
375 heterogeneity in two-dimensional space. Based on the low-dimensional embedding space of UMAP,
376 clustering methods were deployed to define clusters of the data points (**Figure 4d** and **Figure 5e**). The
377 biological significance of resulting clusters was validated by subsequent exploration and evaluation
378 (**Figure 4** and **Figure 6**). For scRNA-seq data, clustering algorithm is generally applied on low-
379 dimensional space, for example in the commonly used scRNA-seq package *Seurat* [57], a graph-based
380 clustering algorithm to low dimensional space by PCA projection. The rationale of applying clustering
381 method to low-dimensional projected space mainly arises from the curse of dimensionality [56]. When
382 computing distance (e.g., Euclidean distance) in high-dimensional data, the difference in the distances
383 between different pairs of samples becomes less precise, which hinders discriminating near and far
384 points. Thus, applying clustering methods to low-dimensional embedding space is better to define
385 clusters of data points. Therefore, we suggest that UMAP can be applied as a pre-processing step
386 before generating clusters from bulk transcriptomic datasets.

387 Although UMAP has shown significant advantages in detecting among-sample heterogeneity. PCA
388 has a unique property not present by other methods. PCA compresses the data by top-ranked principal
389 components and computes the PCA score for each sample. Therefore, it can calculate the variable
390 weight corresponding to new coordinate system (PCA loadings), which explains the contribution of
391 each variable to sample points. In contrast, the nonlinear methods, including MDS, t-SNE and UMAP,
392 do not involve the variable weight such that dimensionality reduction embedding cannot be
393 immediately explainable by variable weight. This might represent an area for the future improvement
394 of UMAP or methods of similar kind.

395 Though commonly used for scRNA-seq, UMAP has been repurposed in large scale genotype datasets
396 to explore the fine structure and visualise genetic interactions [59, 60]. Based on the quantitative and
397 qualitative results of the comparison among dimensionality reduction methods, we highly recommend
398 UMAP as the visualisation tool in the pipeline for bulk transcriptomic profiling and DGE analysis. It
399 can particularly reinforce sample heterogeneity analysis for datasets with large sample sizes.

400
401
402
403

404 **Methods**

405 Datasets

406 The total RNA datasets were collected from the Gene Expression Omnibus (GEO) database with query
407 conditions set as follows: the dataset type was expression profiling by array or by high throughput
408 sequencing; the number of samples ranged from 100 to 10,000; organism was homo sapiens; the
409 publication date was from 2015/01/01 to 2020/03/01; sample source was PBMC or whole blood.
410 Applying the query to the GEO database, we gained 214 results. We further manually removed the
411 datasets in which each group owned less than 100 samples, resulting in 71 datasets.

412

413 Clustering accuracy (NMI, ARI)

414 For clustering accuracy analysis, we applied five clustering methods to the embedded low-dimensional
415 space by dimensionality reduction methods. The clustering methods included k-means clustering
416 (Python function *KMeans*), hierarchical clustering (Python function *AgglomerativeClustering*),
417 spectral clustering (Python function *SpectralClustering*), hdbscan (Python function *hdbscan*) and
418 Gaussian mixture model (Python function *GaussianMixture*). In these clustering methods, the number
419 of clusters k was set to be the known number of different groups in the data, except for hdbscan which
420 is a density-based clustering algorithm (we set the *min_cluster_size* as 10). We applied the five
421 clustering methods to the embedded space of 26 datasets with available features for groups. The
422 retained partitions inferred using the low-dimensional components were compared to the true clusters.
423 The level of agreement between the clustering partition and the true clusters was measured by two
424 criteria: the Adjusted Rand Index (ARI) [39] and the Normalized Mutual Information (NMI) [38].

425 Given two partitions $X = \{X_1, \dots, X_r\}$ and $Y = \{Y_1, \dots, Y_s\}$, the ARI and NMI are defined as:

$$426 \text{ARI}(X, Y) = \frac{\sum_{ij} \binom{n_{ij}}{2} - [\sum_i \binom{a_i}{2} \sum_j \binom{b_j}{2}] / \binom{n}{2}}{\frac{1}{2} [\sum_i \binom{a_i}{2} + \sum_j \binom{b_j}{2}] - [\sum_i \binom{a_i}{2} \sum_j \binom{b_j}{2}] / \binom{n}{2}} \text{ and } \text{NMI}(X, Y) = \frac{2 \text{MI}(X, Y)}{\text{H}(X) + \text{H}(Y)}$$

427 where $n_{ij} = |X_i \cap Y_j|$ is the number of common data points between X_i and Y_j , $a_i = \sum_j n_{ij}$, $b_j =$
428 $\sum_i n_{ij}$, $\text{MI}(X, Y)$ is the mutual information between cluster labels X and Y , $\text{H}(X)$ and $\text{H}(Y)$ are the
429 entropy function for cluster labelling. We used Python function *adjusted_rand_score* and
430 *normalized_mutual_info_score* to calculate ARI and NMI, respectively.

431

432 Neighbourhood preserving evaluation

433 The evaluation of neighbourhood preserving is to assess how the reduced low-dimensional space
434 retains the local information compared with the original high dimensional dataset. For the original
435 space and embedded space, the k-nearest neighbours (kNNs) for each data point were computed

436 respectively (denoted as sets X and Y). The Jaccard index (JI) [40] was used to calculate the
437 neighbourhood similarity between original and embedded space: $JI = |X \cap Y| / |X \cup Y|$ where $|\cdot|$ means set
438 cardinality, then the average Jaccard index (AJI) across all data points were computed to measure the
439 neighbourhood preserving.

440

441 Running time

442 We measured the running time of PCA, MDS, t-SNE and UMAP on a single thread of an Intel Xeon
443 E5-2698 v4 2.20GHz processor. The running time was determined in R using the “elapsed” (wall clock)
444 time measurements, which allows for consistent timing across methods. For total-RNA datasets, the
445 number of samples is moderately large with hundreds of data points. We generated datasets with
446 sample size ranging from 200 to 10000 by random sampling to evaluate the computation efficiency.
447 The data were generated by randomly sampling with replacement from the three largest datasets
448 (GSE36382, GSE65391 and GSE65907).

449

450 Separability of batch effects and biological groups

451 To evaluate the capability of each dimensionality reduction method in separating the groups by the
452 embeddings, we first assigned batch labels to 3 datasets and biological group labels to 9 datasets. For
453 each dataset, we used Python function *train_test_split* with parameter *test_size = 0.3* to divide the
454 dataset into 70% training set and 30% test set. For each algorithm, a random-forest classifier by Python
455 function *RandomForestClassifier* was trained using the group labels as target variable and the
456 embedding's coordinates as training variables. We then utilized these classifiers to predict cluster
457 identities on the test set and computed the accuracy of these predictions, thus assessing the ability of
458 each method to separate groups.

459

460 Statistical test

461 We applied two-tailed t-test to compare the performance of dimensionality reduction methods. The
462 frequency difference of categorical variables was examined by χ^2 test. The p-value less than 0.05 is
463 considered statistically significant. We used R (3.6.3) package *limma* [11, 13] for differential gene
464 expression (DGE) analysis. Top 100 differential expressed genes were chosen to be included in the
465 heatmap among control and experimental groups. We applied gene set enrichment analysis (GSEA)
466 by R package *EGSEA*, where the Molecular Signatures Database (MSigDB) was set as H: hallmark
467 gene sets [61].

468

469 Data availability

470 The datasets supporting the conclusions of this article are available in Gene Expression Omnibus
471 repository (<https://www.ncbi.nlm.nih.gov>) with the GEO accession numbers in **Table S1**, including
472 four columns (UMAP, t-SNE, MDS and PCA) showing which feature information explains the
473 clustering structure of each dataset.

474

475 Code availability

476 All scripts used for dimensionality reduction and clustering are available through Github
477 https://github.com/yuImmuGroup/umap_on_bulk_transcriptomic_analysis; differential gene
478 expression and gene set enrichment analysis are available in
479 https://github.com/yuImmuGroup/transcriptomic_analysis_DGE_and_GSEA.

480

481

482

483 **References**

- 484 1. Heller, M.J., *DNA microarray technology: devices, systems, and applications*. Annual review
485 of biomedical engineering, 2002. **4**(1): p. 129-153.
- 486 2. Lim, E., et al., *Aberrant luminal progenitors as the candidate target population for basal*
487 *tumor development in BRCA1 mutation carriers*. Nature medicine, 2009. **15**(8): p. 907-913.
- 488 3. Wang, Z., M. Gerstein, and M. Snyder, *RNA-Seq: a revolutionary tool for transcriptomics*.
489 *Nature reviews genetics*, 2009. **10**(1): p. 57-63.
- 490 4. Wu, D., et al., *Gene-expression data integration to squamous cell lung cancer subtypes*
491 *reveals drug sensitivity*. British journal of cancer, 2013. **109**(6): p. 1599-1608.
- 492 5. Bombardier, C., et al., *Derivation of the SLEDAI. A disease activity index for lupus patients*.
493 *Arthritis & Rheumatism: Official Journal of the American College of Rheumatology*, 1992.
494 **35**(6): p. 630-640.
- 495 6. Leek, J.T., et al., *Tackling the widespread and critical impact of batch effects in high-*
496 *throughput data*. Nature Reviews Genetics, 2010. **11**(10): p. 733-739.
- 497 7. MDAndersonCancerCenter, U.A. *TCGA Batch Effects Viewer*. 2020 [cited 2020 1st October];
498 Available from: <https://bioinformatics.mdanderson.org/public-software/tcga-batch-effects/>.
- 499 8. Wold, S., K. Esbensen, and P. Geladi, *Principal component analysis*. Chemometrics and
500 intelligent laboratory systems, 1987. **2**(1-3): p. 37-52.
- 501 9. Torgerson, W.S., *Multidimensional scaling: I. Theory and method*. Psychometrika, 1952.
502 **17**(4): p. 401-419.
- 503 10. Love, M.I., W. Huber, and S. Anders, *Moderated estimation of fold change and dispersion for*
504 *RNA-seq data with DESeq2*. Genome biology, 2014. **15**(12): p. 550.
- 505 11. Ritchie, M.E., et al., *limma powers differential expression analyses for RNA-sequencing and*
506 *microarray studies*. Nucleic acids research, 2015. **43**(7): p. e47-e47.
- 507 12. Robinson, M.D., D.J. McCarthy, and G.K. Smyth, *edgeR: a Bioconductor package for*
508 *differential expression analysis of digital gene expression data*. Bioinformatics, 2010. **26**(1):
509 p. 139-140.
- 510 13. Law, C.W., et al., *RNA-seq analysis is easy as 1-2-3 with limma, Glimma and edgeR*.
511 F1000Research, 2016. **5**.
- 512 14. Tang, F., et al., *mRNA-Seq whole-transcriptome analysis of a single cell*. Nature methods,
513 2009. **6**(5): p. 377-382.
- 514 15. Hwang, B., J.H. Lee, and D. Bang, *Single-cell RNA sequencing technologies and bioinformatics*
515 *pipelines*. Experimental & molecular medicine, 2018. **50**(8): p. 1-14.
- 516 16. Van Buren, E., et al., *TWO-SIGMA: a novel TWO-component SInGle cell Model-based*
517 *Association method for single-cell RNA-seq data*. bioRxiv, 2020: p. 709238.
- 518 17. Maaten, L.v.d. and G. Hinton, *Visualizing data using t-SNE*. Journal of machine learning
519 research, 2008. **9**(Nov): p. 2579-2605.
- 520 18. McInnes, L., J. Healy, and J. Melville, *Umap: Uniform manifold approximation and projection*
521 *for dimension reduction*. arXiv preprint arXiv:1802.03426, 2018.
- 522 19. Becht, E., et al., *Dimensionality reduction for visualizing single-cell data using UMAP*. Nature
523 *biotechnology*, 2019. **37**(1): p. 38-44.
- 524 20. Consortium, G., *The Genotype-Tissue Expression (GTEx) pilot analysis: Multitissue gene*
525 *regulation in humans*. Science, 2015. **348**(6235): p. 648-660.
- 526 21. Tomczak, K., P. Czerwińska, and M. Wiznerowicz, *The Cancer Genome Atlas (TCGA): an*
527 *immeasurable source of knowledge*. Contemporary oncology, 2015. **19**(1A): p. A68.
- 528 22. Lou, J., et al., *Rad18 mediates specific mutational signatures and shapes the genomic*
529 *landscape of carcinogen-induced tumors in vivo*. NAR Cancer, 2021. **3**(1): p. zcaa037.

530 23. Banchereau, R., et al., *Personalized Immunomonitoring Uncovers Molecular Networks that*
531 *Stratify Lupus Patients*. *Cell*, 2016. **165**(6): p. 1548-1550.

532 24. Davenport, E.E., et al., *Discovering in vivo cytokine-eQTL interactions from a lupus clinical*
533 *trial*. *Genome Biol*, 2018. **19**(1): p. 168.

534 25. Figgett, W.A., et al., *Machine learning applied to whole-blood RNA-sequencing data*
535 *uncovers distinct subsets of patients with systemic lupus erythematosus*. *Clin Transl*
536 *Immunology*, 2019. **8**(12): p. e01093.

537 26. Guthridge, J.M., et al., *Adults with systemic lupus exhibit distinct molecular phenotypes in a*
538 *cross-sectional study*. *EClinicalMedicine*, 2020. **20**: p. 100291.

539 27. Hong, S., et al., *Longitudinal profiling of human blood transcriptome in healthy and lupus*
540 *pregnancy*. *J Exp Med*, 2019. **216**(5): p. 1154-1169.

541 28. Oon, S., et al., *A potential association between IL-3 and type I and III interferons in systemic*
542 *lupus erythematosus*. *Clin Transl Immunology*, 2019. **8**(12): p. e01097.

543 29. Toro-Domínguez, D., et al., *Stratification of Systemic Lupus Erythematosus Patients Into*
544 *Three Groups of Disease Activity Progression According to Longitudinal Gene Expression*.
545 *Arthritis Rheumatol*, 2018. **70**(12): p. 2025-2035.

546 30. Dunning, J., et al., *Progression of whole-blood transcriptional signatures from interferon-*
547 *induced to neutrophil-associated patterns in severe influenza*. *Nature immunology*, 2018.
548 **19**(6): p. 625-635.

549 31. Hoang, L.T., et al., *Patient-based transcriptome-wide analysis identify interferon and*
550 *ubiquination pathways as potential predictors of influenza A disease severity*. *PLoS One*,
551 **2014**. **9**(11): p. e111640.

552 32. Zhai, Y., et al., *Host transcriptional response to influenza and other acute respiratory viral*
553 *infections—a prospective cohort study*. *PLoS Pathog*, 2015. **11**(6): p. e1004869.

554 33. Le-Niculescu, H., et al., *Towards precision medicine for stress disorders: diagnostic*
555 *biomarkers and targeted drugs*. *Molecular Psychiatry*, 2020. **25**(5): p. 918-938.

556 34. Narang, V., et al., *Influenza vaccine-induced antibody responses are not impaired by frailty in*
557 *the community-dwelling elderly with natural influenza exposure*. *Frontiers in immunology*,
558 **2018**. **9**: p. 2465.

559 35. Rawat, C., et al., *Downregulation of peripheral PTGS2/COX-2 in response to valproate*
560 *treatment in patients with epilepsy*. *Scientific reports*, 2020. **10**(1): p. 1-14.

561 36. Tasaki, S., et al., *Multi-omics monitoring of drug response in rheumatoid arthritis in pursuit*
562 *of molecular remission*. *Nature communications*, 2018. **9**(1): p. 1-12.

563 37. Thakar, J., et al., *Aging-dependent alterations in gene expression and a mitochondrial*
564 *signature of responsiveness to human influenza vaccination*. *Aging (Albany NY)*, 2015. **7**(1):
565 p. 38.

566 38. Danon, L., et al., *Comparing community structure identification*. *Journal of Statistical*
567 *Mechanics: Theory and Experiment*, 2005. **2005**(09): p. P09008.

568 39. Rand, W.M., *Objective criteria for the evaluation of clustering methods*. *Journal of the*
569 *American Statistical association*, 1971. **66**(336): p. 846-850.

570 40. Levandowsky, M. and D. Winter, *Distance between sets*. *Nature*, 1971. **234**(5323): p. 34-35.

571 41. Leek, J.T., et al., *The sva package for removing batch effects and other unwanted variation in*
572 *high-throughput experiments*. *Bioinformatics*, 2012. **28**(6): p. 882-3.

573 42. Risso, D., et al., *Normalization of RNA-seq data using factor analysis of control genes or*
574 *samples*. *Nature biotechnology*, 2014. **32**(9): p. 896-902.

575 43. Gerstner, J.R., et al., *Removal of unwanted variation reveals novel patterns of gene*
576 *expression linked to sleep homeostasis in murine cortex*. BMC genomics, 2016. **17**(8): p. 377-
577 387.

578 44. Obeidat, M.e., et al., *The effect of different case definitions of current smoking on the*
579 *discovery of smoking-related blood gene expression signatures in chronic obstructive*
580 *pulmonary disease*. Nicotine & Tobacco Research, 2016. **18**(9): p. 1903-1909.

581 45. NIH. *Systemic Lupus Erythematosus (Lupus)*. 2020 [cited 2020 1st October]; Available from:
582 <https://www.niams.nih.gov/health-topics/lupus>.

583 46. Buyon, J.P., et al., *The effect of combined estrogen and progesterone hormone replacement*
584 *therapy on disease activity in systemic lupus erythematosus: a randomized trial*. Annals of
585 internal medicine, 2005. **142**(12_Part_1): p. 953-962.

586 47. Toro-Domínguez, D., et al., *Stratification of systemic lupus erythematosus patients into*
587 *three groups of disease activity progression according to longitudinal gene expression*.
588 Arthritis & Rheumatology, 2018. **70**(12): p. 2025-2035.

589 48. Alhamdoosh, M., et al., *Combining multiple tools outperforms individual methods in gene set*
590 *enrichment analyses*. Bioinformatics, 2017. **33**(3): p. 414-424.

591 49. Munoz, L.E., et al., *The role of defective clearance of apoptotic cells in systemic*
592 *autoimmunity*. Nature Reviews Rheumatology, 2010. **6**(5): p. 280.

593 50. Banchereau, J. and V. Pascual, *Type I interferon in systemic lupus erythematosus and other*
594 *autoimmune diseases*. Immunity, 2006. **25**(3): p. 383-392.

595 51. Ivashkiv, L.B., *IFNy: signalling, epigenetics and roles in immunity, metabolism, disease and*
596 *cancer immunotherapy*. Nature Reviews Immunology, 2018. **18**(9): p. 545-558.

597 52. Holland, S.M., *Principal components analysis (PCA)*. Department of Geology, University of
598 Georgia, Athens, GA, 2008: p. 30602-2501.

599 53. Borg, I. and P.J. Groenen, *Modern multidimensional scaling: Theory and applications*. 2005:
600 Springer Science & Business Media.

601 54. Preparata, F.P. and M.I. Shamos, *Computational geometry: an introduction*. 2012: Springer
602 Science & Business Media.

603 55. Kobak, D. and G.C. Linderman, *UMAP does not preserve global structure any better than t-*
604 *SNE when using the same initialization*. bioRxiv, 2019.

605 56. Kriegel, H.-P., P. Kröger, and A. Zimek, *Clustering high-dimensional data: A survey on*
606 *subspace clustering, pattern-based clustering, and correlation clustering*. ACM Transactions
607 on Knowledge Discovery from Data (TKDD), 2009. **3**(1): p. 1-58.

608 57. Butler, A., et al., *Integrating single-cell transcriptomic data across different conditions,*
609 *technologies, and species*. Nature biotechnology, 2018. **36**(5): p. 411-420.

610 58. Sun, S., et al., *Accuracy, robustness and scalability of dimensionality reduction methods for*
611 *single-cell RNA-seq analysis*. Genome biology, 2019. **20**(1): p. 269.

612 59. Dorrrity, M.W., et al., *Dimensionality reduction by UMAP to visualize physical and genetic*
613 *interactions*. Nature communications, 2020. **11**(1): p. 1-6.

614 60. Sakaue, S., et al., *Dimensionality reduction reveals fine-scale structure in the Japanese*
615 *population with consequences for polygenic risk prediction*. Nature communications, 2020.
616 **11**(1): p. 1-11.

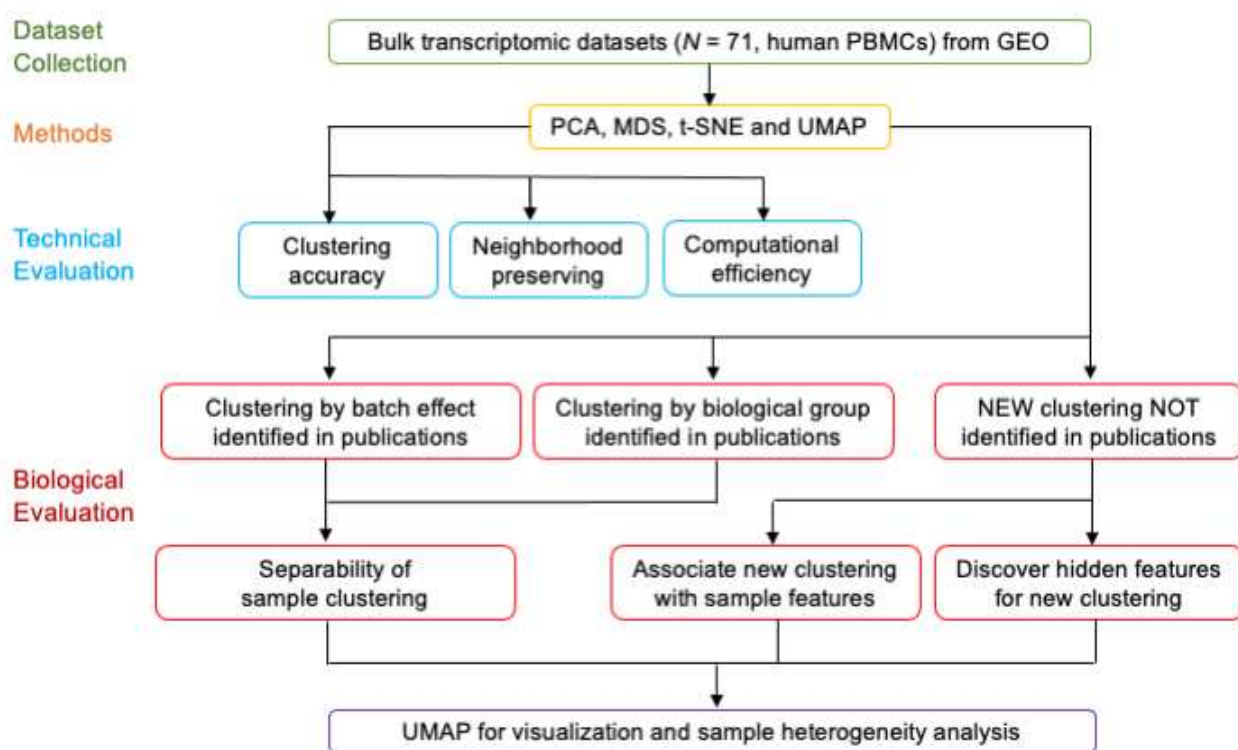
617 61. Liberzon, A., et al., *The molecular signatures database hallmark gene set collection*. Cell
618 systems, 2015. **1**(6): p. 417-425.

619

620

Figure 1

a Schematic overview.



b

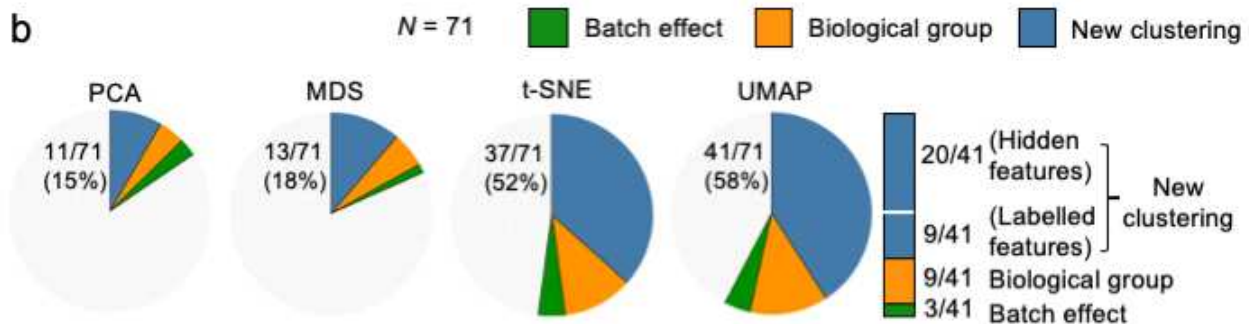


Figure 2

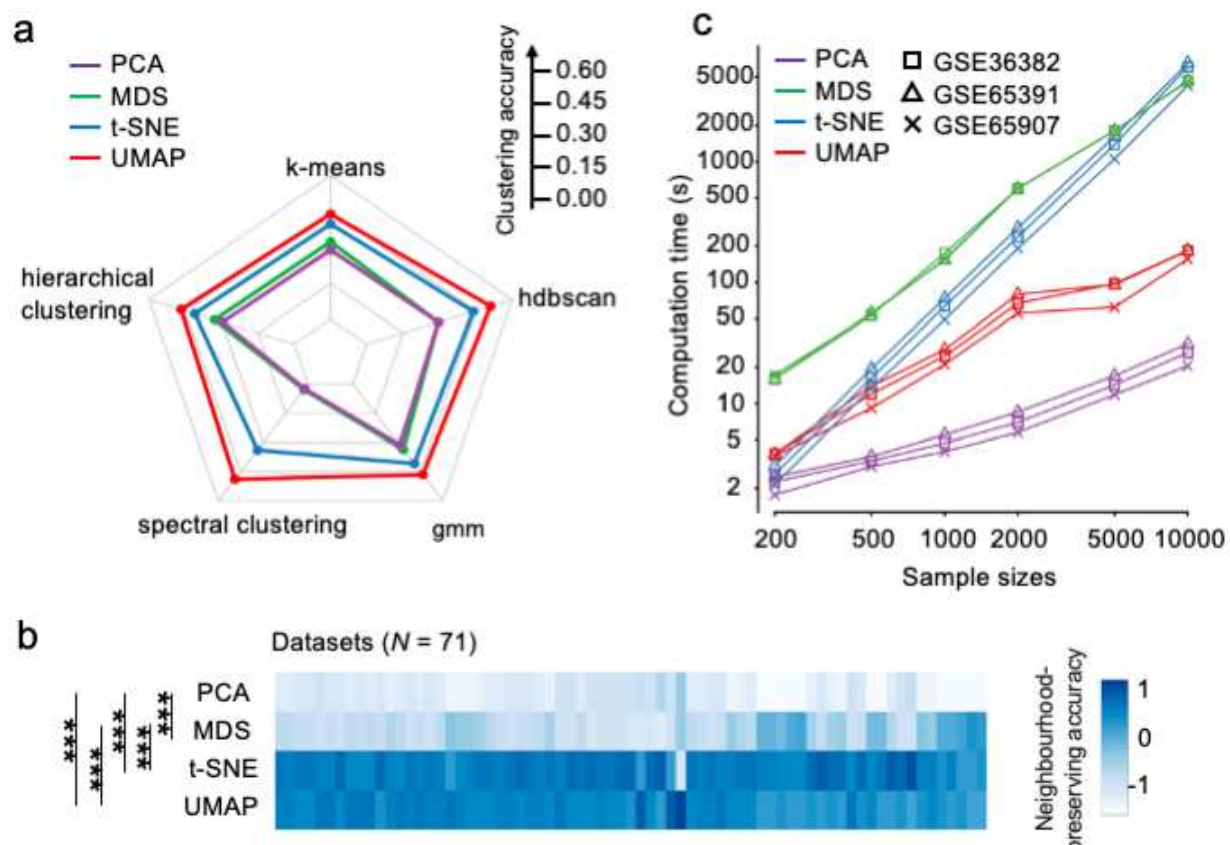


Figure 3

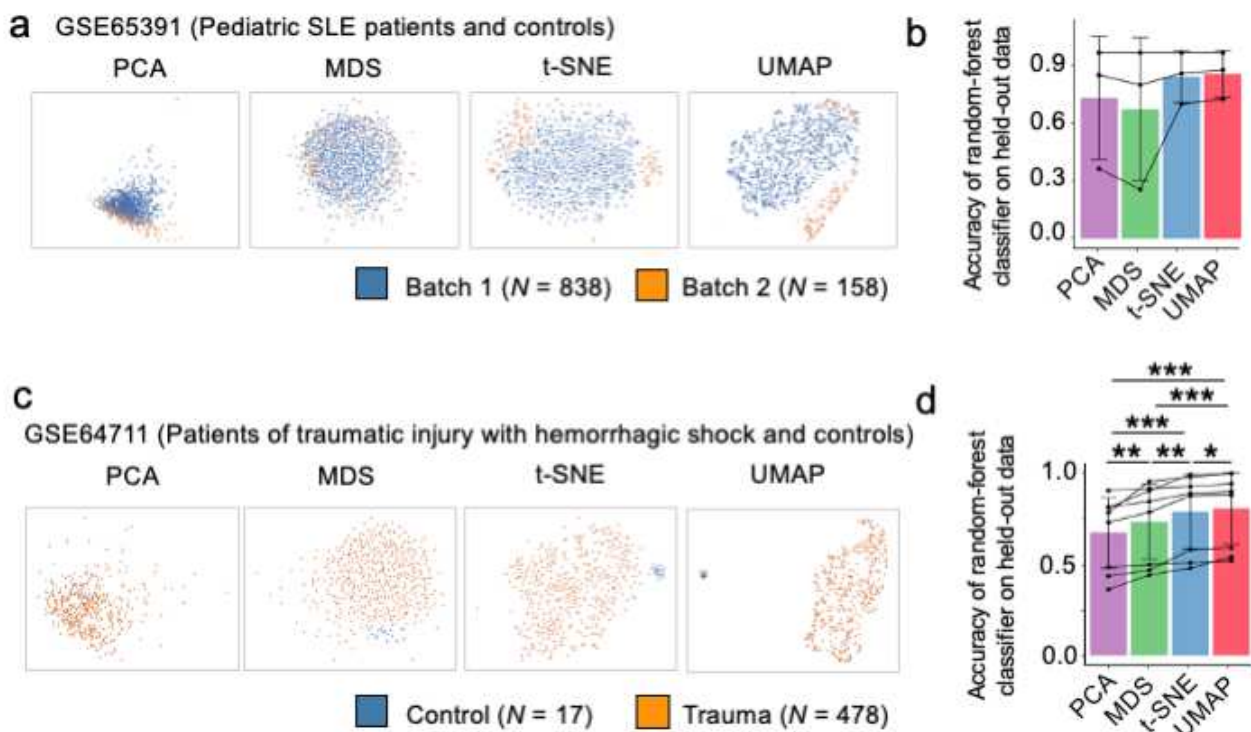
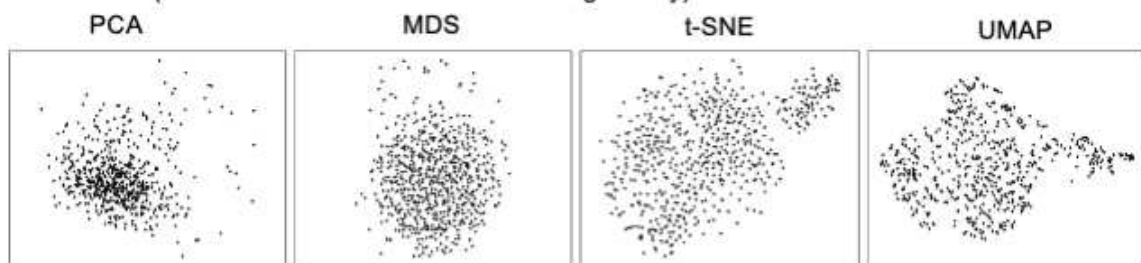
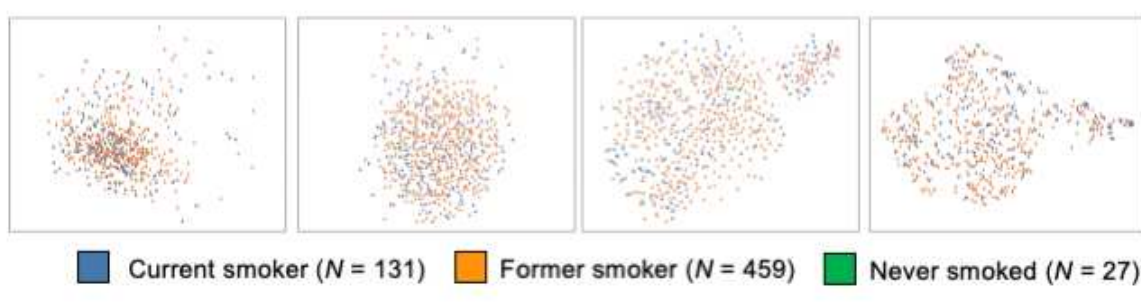


Figure 4

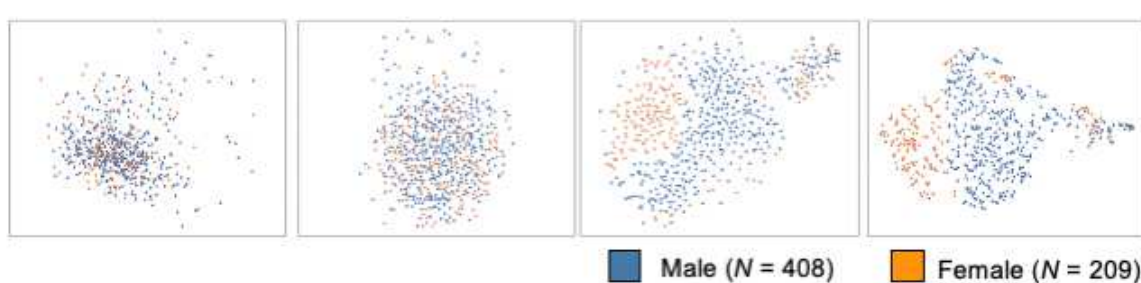
a GSE71220 (COPD Patients with different smoking history)



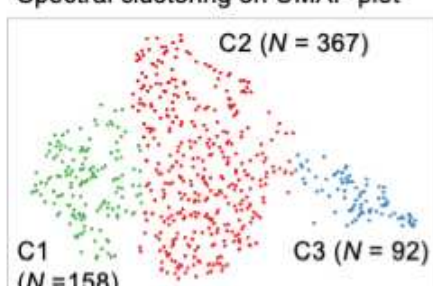
b



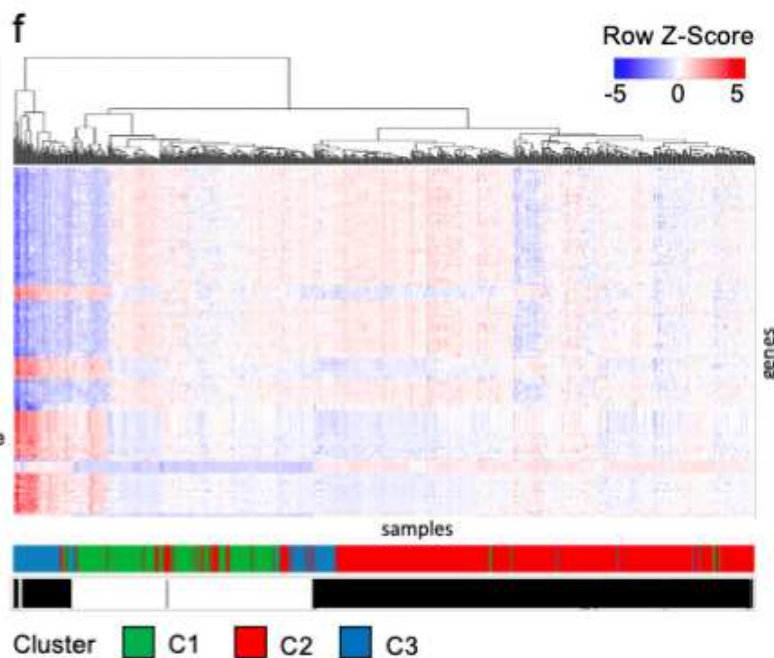
c



d Spectral clustering on UMAP plot



f



e

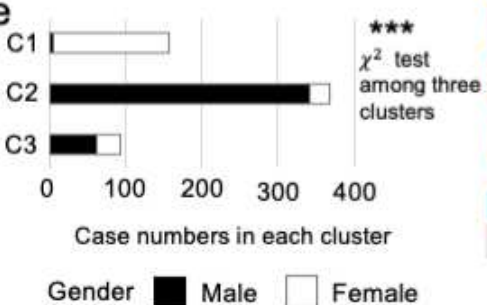
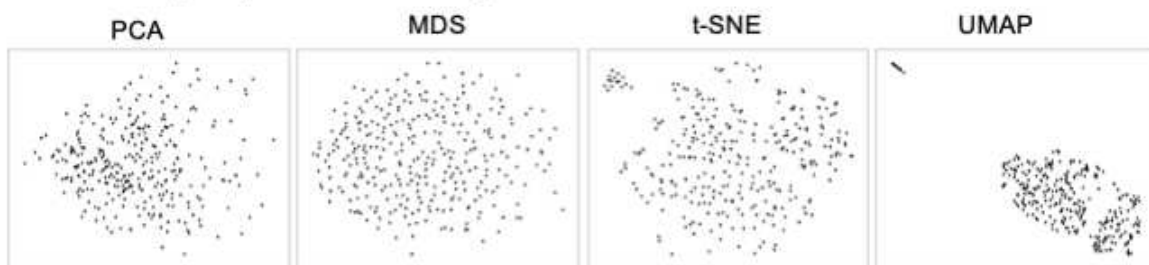
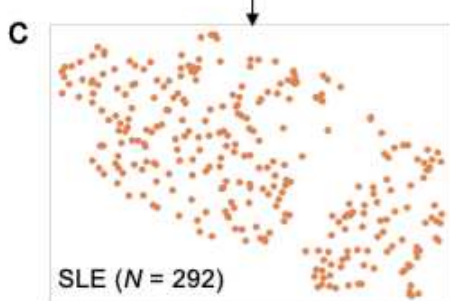
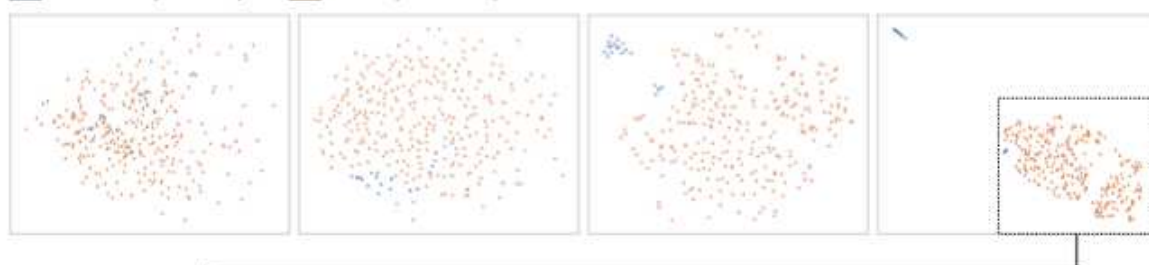


Figure 5

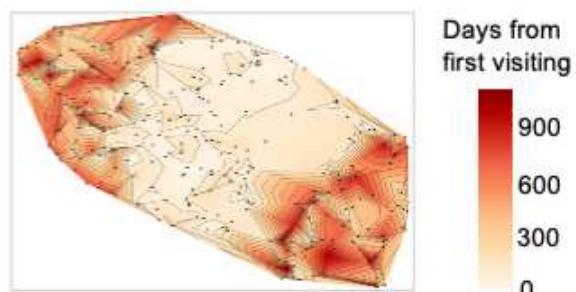
a GSE121239 (SLE patients and controls)



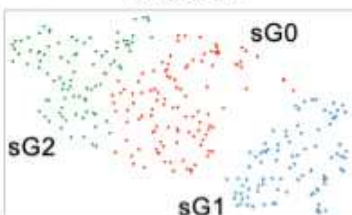
b Control ($N = 20$) SLE ($N = 292$)



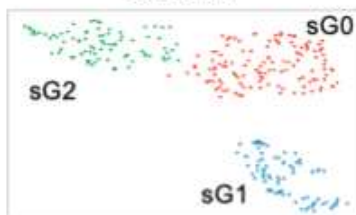
d



e euclidean



canberra



cosine

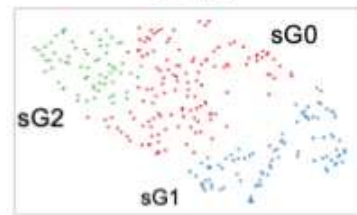


Figure 6

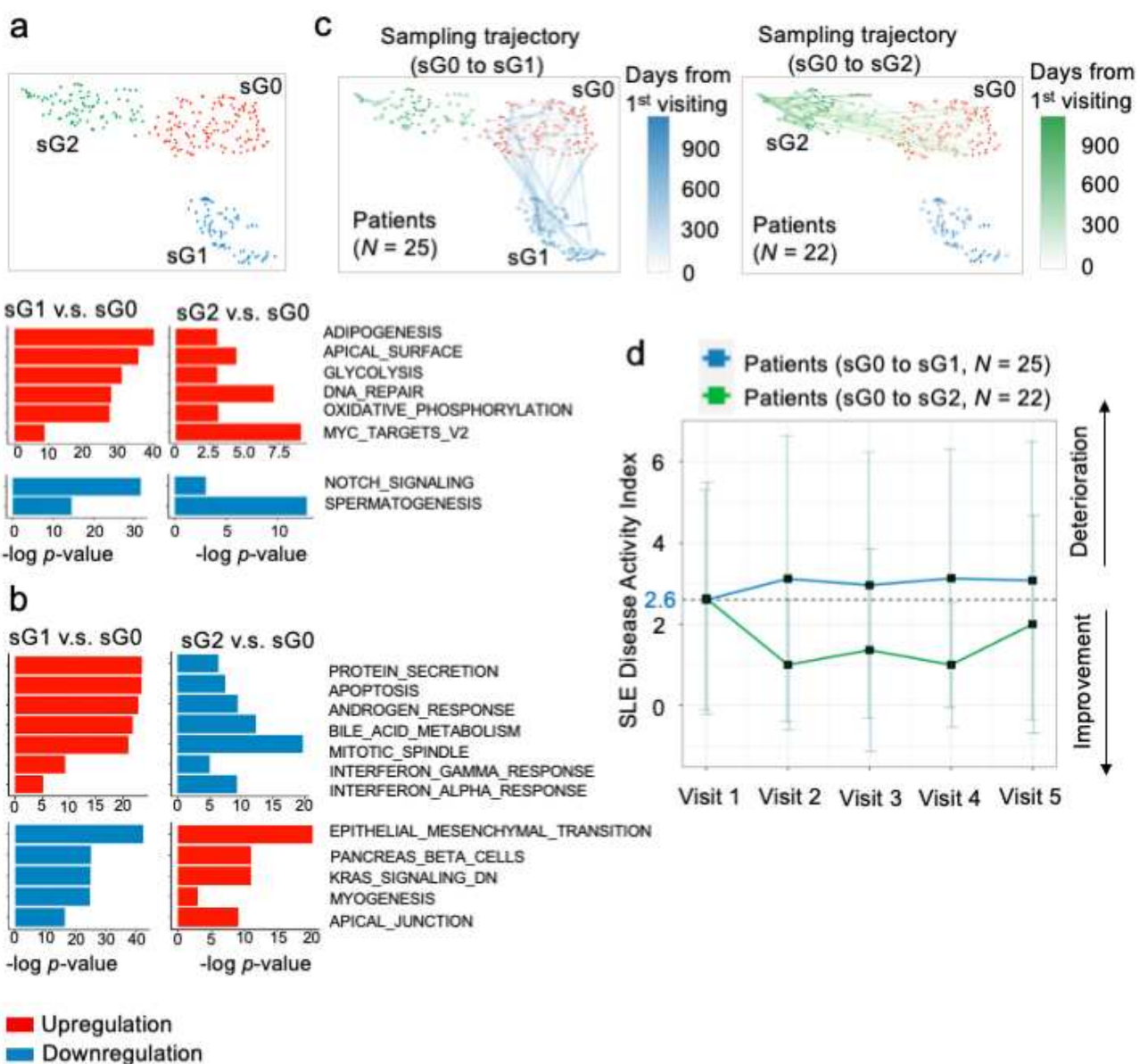
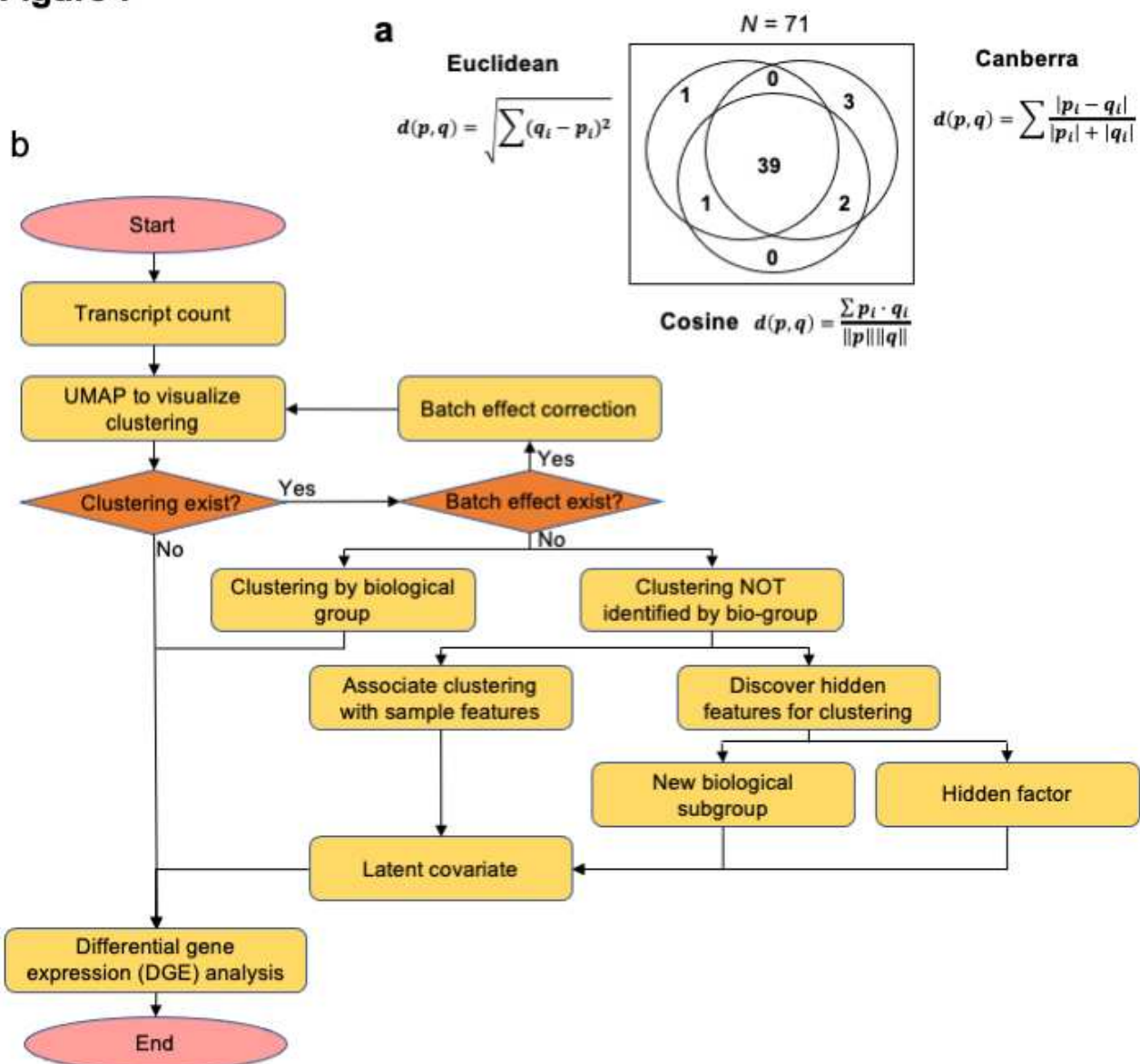


Figure 7



628 **Figure Legends**

629 **Figure 1. Evaluation overview for four dimensionality reduction methods.**

630 (a) Schematic overview of the evaluation. Bulk transcriptomic datasets were collected from GEO
631 database, followed by applying four methods to the datasets for visualization. The methods were
632 evaluated in both technical and biological aspects. Finally, we presented the recommendation on
633 UMAP for visualization.

634 (b) Pie chart showing the percentage of datasets by biological explanations for all revealed clustering
635 structures.

636 By associating features identified in publications, clustering structures were divided into three
637 categories: batch effect (coloured green), biological group (coloured orange) and new clustering
638 (coloured blue). Batch effect was the cluster associated with batch effects. Biological group was related
639 to experimental design like control and treatment groups, while new clustering was the clusters related
640 to other predefined features like gender. New clustering was further divided into new clustering with
641 sample features and new clustering with hidden features by considering available feature information.

642

643 **Figure 2.**

644 **Quantitative analysis of four dimensionality reduction methods.**

645 (a) Radar plot of clustering accuracy (average NMI score) comparison using five clustering methods
646 on 22 datasets with cluster labels. The input was the embedded two-dimensional coordinates of
647 each dimensionality reduction methods. Larger scale denotes better clustering accuracy.

648 (b) Heatmap for evaluating neighbourhood preserving of each method on 71 datasets. The number of
649 neighbours is set as 15. The darker the colour is, the better the local information is retained. One-
650 way ANOVA shows significant difference among the four methods (**p<0.001). R function
651 *heatmap* in R package *stats* was used for Figure 2b.

652 (c) Running time evaluation of four dimensionality reduction methods with varying sample sizes. Log-
653 transforming of the time was applied. Different sizes of data were generated by sampling with
654 replacement from three largest datasets respectively.

655

656 **Figure 3. Biological explanation of clustering by batch effects and biological group.**

657 (a) Visualization of dataset GSE65391 showing the batch effects (coloured by blue and orange) in
658 two-dimensional space by dimensionality reduction methods.

659 (b) Visualization of dataset GSE55447 illustrating biological group by dimensionality reduction
660 methods. Control group is labelled in blue and trauma group is in orange.

661 (c), (d) Classification accuracy on held-out data of random-forest classifiers predicting cluster labels
662 taking embedded coordinates as input. (c) is for batch effects, while (d) for biological groups. The
663 average score across datasets is shown, with vertical bars representing s.d.; paired t-test was conducted
664 on pairwise methods (* p < 0.05, ** p < 0.01, *** p < 0.001)

665

666 **Figure 4.**

667 **New clustering interpreted by available sample features.**

668 (a)-(c) Visualization of dataset GSE71220 in two-dimensional space by assigning no feature (a), group
669 labels (b), gender (c).

670 (d) Spectral clustering on two-dimensional embedded coordinates into three clusters: C1, C2, C3.

671 (e) Gender proportion among three clusters by χ^2 test showing a significant difference (***(p < 0.001)).

672 Male and female are coloured by black and white respectively.

673 (f) Heatmap of top-100 differentially expressed genes with three clusters C1, C2, C3 and two gender
674 groups male and female. R function *heatmap.2* in R package *gplots* was used for Figure 4f.

675

676 **Figure 5. Discovering new associations between clustering structures and hidden features.**

677 (a), (b) Visualization of dataset GSE121239 in two-dimensional space by assigning no feature (a),
678 group labels (b).

679 (c) Patient (SLE) group (coloured orange) showing new clustering structure (sG1, lower right).

680 (d) Contour plot on patient groups by the order of visiting timestamp. Each data point is associated
681 with one visiting timestamp. Data points are coloured by the order of visiting time with light colours
682 for early visits and dark colour for late visits. The code to plot Figure 5d is in Code Availability.

683 (e) Hierarchical clustering of patient group on two-dimensional embedded coordinates by UMAP with
684 distance metric as 'euclidean', 'canberra', and 'cosine', respectively.

685

686 **Figure 6. UMAP revealed clustering structure explained by clinical traits.**

687 (a) Hierarchical clustering of patient groups on two-dimensional embedded coordinates by UMAP
688 with metric as 'canberra'.

689 (b) Histogram illustrating gene set enrichment analysis between sG1 v.s. sG0 and sG2 v.s. sG0 with
690 top 20 differentially regulated molecular pathways (negative logarithm of the p-value (base 10)).
691 Colour red denotes upregulation and blue for downregulation. The top two rows are the same
692 direction of regulation, and the bottom two rows are in the opposite direction.

693 (c) Visiting trajectories of each patient on UMAP plot with metric = 'canberra'. Each path connected
694 data points corresponding to one patient with several visits. Data points in paths were connected

695 by visiting timestamp. The light colour denotes early visit and dark colour for late visits. The paths
696 were mainly divided into two patterns: from sG0 to sG1, from sG0 to sG2.

697 (d) Line chart of average SLEDAI changing along with visits between sG0 to sG1 and sG0 to sG1.
698 Both started with average SLEDAI around 2.6; from sG0 to sG1 (coloured by blue) the average
699 SLEDAI increased, while from sG0 to sG2 (coloured by green) the average SLEDAI decreased.

700

701 **Figure 7.**

702 **Recommendations for UMAP processing bulk transcriptome datasets.**

703 (a) Venn diagram illustrating the overlap in the number of datasets having clustering structure by the
704 UMAP plot under three different '*metric*' parameters: '*euclidean*', '*canberra*', and '*cosine*'.
705 (b) The recommendation pipeline for applying UMAP to bulk transcriptome analysis.

706